A Physical-Layer Network Coding Scheme Based on Linear MIMO Detection

Hao-Hsiang Chung, Shiuan-Hao Kuo
Graduate Institute of Communication Engineering
National Taiwan University
Taipei, Taiwan
E-mail: {d94942020, d96942022}@ntu.edu.tw

Mao-Chao Lin
Dept. of Electrical Engineering
National Taiwan University
Taipei, Taiwan
E-mail: mclin@cc.ee.ntu.edu.tw

***Abstract*—A physical-layer network coding (PNC) scheme based on MIMO linear detection is proposed in this paper for a two-way relay channel with a multi-antenna relay. We apply a real-valued linear combiner to the output symbols of the MIMO linear detector to obtain a superimposed constellation for which the labelling is obtained from the exclusive or operation on the two transmitted symbols. The superimposed constellation is QAM-like which can facilitate the SER (symbol error rate) analysis.**

I. Introduction

Network coding (NC) is proved to be a promising tool to increase network throughput [1]. Instead of simply forwarding data, an intermediate node may do some calculation (coding) on its input packets and send the result, while end nodes can resolve the desired information from those network-coded packets.

Consider a wireless two-way relay channel (TWRC), where two end nodes are intended to exchange information to each other through a relay. For each exchange, four time slots are needed which include two needed for the transmissions from the two end nodes to the relay node and another two needed for the transmissions from the relay node to the two end nodes. By employing network coding transmission [2], the two end nodes in turn send their data to the relay, and the relay broadcasts the XORed data to both end nodes. An end node can obtained the other's data by XORing out its own data from the received packet. In this way, only three time slots are needed for each exchange.

In [3], the two-phase physical-layer network coding (PNC) concept is introduced. In the first MA (multiple-access) phase, both end nodes send their data to the relay simultaneously. The relay detects the desired network-coded packet directly using the superimposed signal. In the second BC (broadcast) phase, the relay sends the network-coded data back to the end nodes. The major difference between NC and PNC is the detection method at the relay. In the NC operation, individual packets from two end nodes are detected separately, and then the combination is calculated based on these detected packets. In the PNC operation, the relay does not individually detect the packet of each end node. Instead, the desired network-coded packet is calculated directly through the superimposed data sent simultaneously from the two end nodes. This direct calculation process improves the throughput by one time slot as compared to its NC counterpart.

Recently, research which combines two-way relay and MIMO is emerging, e.g. MIMO-NC [4] and MIMO-PNC [5]. In MIMO-NC, network coding is combined with MIMO where the relay is equipped with multiple antennas. The individual packets from the two end nodes can be detected by the traditional MIMO linear detection, e.g., zero forcing (ZF) or minimum mean square error (MMSE) detectors. Therefore, the network-coded symbols can be generated accordingly. Since we are interested in network-coded symbols at the relay, there is no need to detect the packet of individual end node. This is the main concept of PNC. MIMO-PNC [5] is a PNC scheme in which the network-coded symbols are recovered directly from the sum and difference of its two end nodes' symbols, and LLR combination is also proposed to combine the information resides in the sum and difference of the symbols.

In this paper, we consider a PNC scheme in TWRC with a multi-antenna relay. This scheme is based on MIMO linear detection. We introduce a real-valued linear combiner with the parameter $\boldsymbol{a} = [a_1 \ a_2]$. If $\mathcal{X}_1$ and $\mathcal{X}_2$ denote the constellation from the two end nodes, the superimposed constellation which we are dealing with is $a_1\mathcal{X}_1+a_2\mathcal{X}_2$. The resulting constellation has a square QAM-like shape, which not only facilitates SER (symbol error rate) analysis, but also can be optimized for improving the error rates. We also provide a simple method to find an optimized $\boldsymbol{a}$.

This paper is organized as follows: In Section II, the system model is shown. In Section III, the proposed PNC mapping scheme is presented in detail. In Section IV, we show the simulation results. Finally, we give the conclusion in Section V.

II. System Model

A. Two-way Relay Channel

Consider a two-way relay channel as shown in Fig. 1. The two end nodes, N_1 and N_2, exchange information through the relay node R. There is no direct link between N_1 and N_2. All nodes are half-duplex, i.e., a node can not transmit and receive simultaneously. In this paper, we discuss the MIMO relay case for which the relay has two antennas and each of the two end nodes has a single antenna.

978-1-4673-0990-5/12/$31.00 ©2012 IEEE

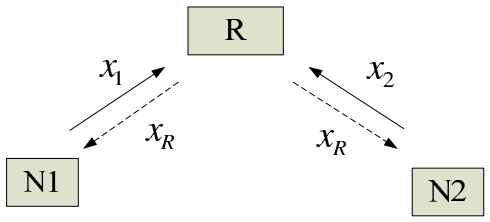

Fig. 1. Two-phase PNC transmission in a two way relay channel.

A PNC transmission [3], [6] consists of two phases. In the first phase which is the MA (multiple-access) phase, both end nodes transmit their information to the relay simultaneously. We assume a symbol level synchronization at the relay. The received signal can be written as

$$\boldsymbol{y}_R = \boldsymbol{H}\boldsymbol{x} + \boldsymbol{z}, \tag{1}$$

where $\boldsymbol{x} = [x_1\ x_2]$ and x_j, $j = 1, 2$ is the transmitted signal from node-j. The channel matrix $\boldsymbol{H}$ can be shown as a 2×2 MIMO channel

$$\boldsymbol{H} = \begin{bmatrix} h_{11} & h_{12} \\ h_{21} & h_{22} \end{bmatrix},$$

where h_{ij} denotes the channel from node-j to the i-th antenna of the relay and $\boldsymbol{z} = [z_1\ z_2]$ is the Gaussian distributed noise with $z_i \sim \mathcal{CN}(0, N_0)$, $i = 1, 2$. We assume a slow block fading and perfect channel information at the receiver.

Denote $\mathcal{M}$ as the mapper used by the two end nodes at the MA phase. For example, if QPSK is used, $x_j = \mathcal{M}(\boldsymbol{b}_j) \in \mathcal{X}$ where $\boldsymbol{b}_j$ is the binary two-tuple to be mapped to x_j and $\mathcal{X}$ is the set of points from the QPSK constellation.

The relay uses a denoising function to map its received signal to a binary two-tuple $\boldsymbol{b}_R$, which is an estimate of $\boldsymbol{b}_1 \oplus \boldsymbol{b}_2$. After estimating the XORed value, in the second phase which is the BC (broadcast) phase, the relay maps $\boldsymbol{b}_R$ to a symbol $\boldsymbol{x}_R$ and then broadcasts it to both end nodes. For simplicity, the relay's mapper $\mathcal{M}_R$ is chosen as the same with the one used in node 1 and 2, i.e., $\mathcal{M}_R = \mathcal{M}$. The received signals of node 1 and 2 are

$$y_1 = \boldsymbol{h}_1\boldsymbol{x}_R + z_1$$
$$y_2 = \boldsymbol{h}_2\boldsymbol{x}_R + z_2,$$

where $\boldsymbol{h}_j$, $j = 1, 2$ are channels from the relay to node j. The end node N_1 can resolve the transmitted information of the end node N_2 by the result of the XOR operation of $\boldsymbol{b}_1$ and the estimate of $\boldsymbol{x}_R$. Similarly, N_2 can resolve the transmitted information of N_1.

III. PNC Mapping

A. Linear MIMO detection

In an MIMO spatial-multiplexing (SM) system, the operation of linear detection followed by quantization [7] is simple and the complexity of estimating the transmitted data is low. Assume the received signal is $\boldsymbol{y}_R = \boldsymbol{H}\boldsymbol{x} + \boldsymbol{z}$, the estimate is obtained by first multiplying an detector matrix $\boldsymbol{G}$,

$$\boldsymbol{G}\boldsymbol{y}_R = \boldsymbol{G}\boldsymbol{H}\boldsymbol{x} + \boldsymbol{G}\boldsymbol{z}. \tag{2}$$

Then $\boldsymbol{G}\boldsymbol{y}_R$ is quantized in a component-wise way according to the mapper from the transmitter. Let $\hat{\boldsymbol{x}}$ be the resulting estimate of the transmitted symbol $\boldsymbol{x}$, the binary transmitted information can be obtained as

$$\hat{\boldsymbol{b}}_j = \mathcal{M}^{-1}(\hat{x}_j), \tag{3}$$

where $\mathcal{M}$ is the mapper, $\hat{x}_j$ is the j-th component of $\hat{\boldsymbol{x}}$, and $\hat{\boldsymbol{b}}_j$ is the binary tuple.

Two major detectors, i.e., *zero forcing* (ZF) and *minimum mean squared error* (MMSE) respectively can be used. The ZF detector is obtained by setting $\boldsymbol{G}$ as the pseudo-inverse of $\boldsymbol{H}$,

$$\boldsymbol{G} = \boldsymbol{H}^{\dagger} = (\boldsymbol{H}^*\boldsymbol{H})^{-1}\boldsymbol{H}^*. \tag{4}$$

The MMSE detector is obtained by minimizing the mean square error as

$$\boldsymbol{G} = \arg\min_{\boldsymbol{G}'} \|\boldsymbol{G}'\boldsymbol{y}_R - \boldsymbol{x}\|^2 \tag{5}$$
$$= (\boldsymbol{H}^*\boldsymbol{H} + N_0\boldsymbol{I})^{-1}\boldsymbol{H}^*. \tag{6}$$

Generally, a MMSE detector can outperform a ZF one with the price of additional complexity.

B. MIMO-NC scheme

In the MIMO-NC scheme [4], the network-coded packets can be obtained after individual packets from the end nodes are estimated. For example, in our system model, if MMSE is adopted, $\boldsymbol{G}$ is set as in (6). The binary network-coded packet is calculated as

$$\boldsymbol{b}_R = \mathcal{M}^{-1}(\hat{x}_1) \oplus \mathcal{M}^{-1}(\hat{x}_2). \tag{7}$$

Then the relay broadcasts the network-coded signal $\boldsymbol{x}_R = \mathcal{M}_R(\boldsymbol{b}_R)$ to the two end nodes.

C. MIMO-PNC scheme-I

In [5] which is referred as MIMO-PNC scheme-I in this paper, a sum-difference matrix $\boldsymbol{D}$ is introduced to detect the network-coded symbols from a sum/difference signal space. Rewrite (1) as

$$\boldsymbol{y}_R = (\boldsymbol{H}\boldsymbol{D}^{-1})(\boldsymbol{D}\boldsymbol{x}) + \boldsymbol{z} = \tilde{\boldsymbol{H}}\tilde{\boldsymbol{x}} + \boldsymbol{z}, \tag{8}$$

where $\boldsymbol{D} = 2\boldsymbol{D}^{-1} = \begin{bmatrix} 1 & 1 \\ 1 & -1 \end{bmatrix}$. The detection is based on the equivalent channel matrix $\tilde{\boldsymbol{H}}$. For example, the ZF detector $\boldsymbol{G} = (\tilde{\boldsymbol{H}}^*\tilde{\boldsymbol{H}})^{-1}\tilde{\boldsymbol{H}}^*$. The sum-difference data $\tilde{\boldsymbol{x}} = [x_1 + x_2\ \ x_1 - x_2]^T$ can be estimated from the detector, and can be then mapped to the desired network coded symbol. To further enhance the performance, LLR combining is used for the final decision.

D. MIMO-PNC scheme-II

In this section, we show the proposed MIMO-PNC mapping scheme referred in this paper as MIMO-PNC scheme-II.

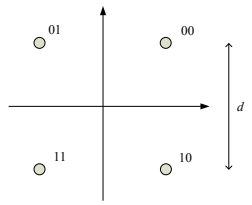

Fig. 2. Constellation of Gray-labelled QPSK, where d is the minimum distance.

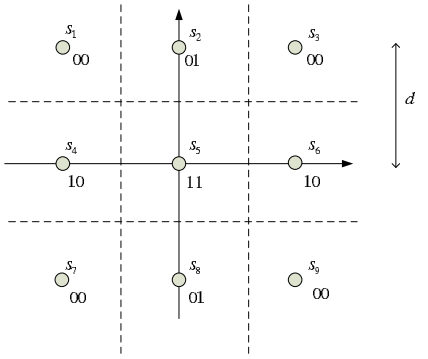

Fig. 3. Superimposed constellation $\boldsymbol{ax}$ for $\boldsymbol{a} = [1\ 1]$, where d is the minimum distance of each component constellation. Each of the two component constellations is the Gray-labelled QPSK constellation shown in Fig. 2.

1) Detection on Superimposed Constellation: In addition to the linear MIMO detector, we introduce a linear combiner $\boldsymbol{a}$ as

$$\boldsymbol{aGy}_R = \boldsymbol{aGHx} + \boldsymbol{aGz}, \tag{9}$$

where $\boldsymbol{a}$ is a 1×2 real-valued vector. The expression (9) can be considered as the simplified channel

$$r = s + n, \tag{10}$$

where $r = \boldsymbol{aGy}_R$, $s = \boldsymbol{aGHx}$, and $n = \boldsymbol{aGz}$. The signal s is located in the superimposed constellation of $\boldsymbol{aGHx}$. In the ZF case, $\boldsymbol{aGHx} = \boldsymbol{ax}$, since $\boldsymbol{G}$ is the pseudo-inverse of $\boldsymbol{H}$. Then, we have $s \in a_1\mathcal{X}_1 + a_2\mathcal{X}_2 = \{a_1x_1 + a_2x_2 | x_1 \in \mathcal{X}_1, x_2 \in \mathcal{X}_2\}$, where $\boldsymbol{a} = [a_1\ a_2]$ and $\mathcal{X}_j$ is the constellation used in node-j. Note that a_1 and a_2 are real numbers. Suppose that $\mathcal{X}_1$ and $\mathcal{X}_2$ are signal points in the constellation of Gray-labelled QPSK symbols as shown in Fig. 2, where d denotes the minimum distance within the points. Then, Fig. 3 shows the superimposed constellation with $\boldsymbol{a} = [1\ 1]$.

In the MMSE case, $\boldsymbol{GH}$ is not exactly equal to $\boldsymbol{I}$. However, the MMSE detector $\boldsymbol{G}$ is obtained by minimizing the mean square error, $\|\boldsymbol{Gy}_R - \boldsymbol{x}\|^2$. Thus, we can still think that s is approximately in $a_1\mathcal{X}_1 + a_2\mathcal{X}_2$.

2) Symbol Error Rate Analysis: Since $\boldsymbol{a}$ is real, the resulting constellation has a square QAM-like shape as shown in Fig. 4. Note that a_1 and a_2 can be any real number, not necessary to be both positive. Let $a_m = \min\{|a_1|, |a_2|\}$ and $a_M = \max\{|a_1|, |a_2|\}$. The distance relationship within the points can be shown in Fig. 4.

The label of each signal point in Fig. 4 is obtained from two components. For example, if a point is obtained from $a_1x_1 + a_2x_2$, where $x_1 = \mathcal{M}(\boldsymbol{b}_1)$ and $x_2 = \mathcal{M}(\boldsymbol{b}_2)$, then its label is $\boldsymbol{b}_1 \oplus \boldsymbol{b}_2$. Since we have four outcomes of a 2-bit label, the points in Fig. 4 can be grouped by four sets according to their labels. Since the two end nodes adopt the same labelling scheme, i.e., Gray-labelled QPSK as shown in Fig. 2, the four groups can be always separated as

$$\begin{aligned}
\boldsymbol{S}_a &= \{s_1, s_4, s_{13}, s_{16}\} \\
\boldsymbol{S}_b &= \{s_2, s_3, s_{14}, s_{15}\} \\
\boldsymbol{S}_c &= \{s_5, s_8, s_9, s_{12}\} \\
\boldsymbol{S}_d &= \{s_6, s_7, s_{10}, s_{11}\},
\end{aligned}$$

where $a, b, c,$ and d represent the four possible labels. We can write the symbol error rate as the sum of its group-wise components as

$$\begin{aligned}
P_e = &P\{\hat{s} \notin \boldsymbol{S}_a | s \in \boldsymbol{S}_a\} P\{s \in \boldsymbol{S}_a\} + \\
&P\{\hat{s} \notin \boldsymbol{S}_b | s \in \boldsymbol{S}_b\} P\{s \in \boldsymbol{S}_b\} + \\
&P\{\hat{s} \notin \boldsymbol{S}_c | s \in \boldsymbol{S}_c\} P\{s \in \boldsymbol{S}_c\} + \\
&P\{\hat{s} \notin \boldsymbol{S}_d | s \in \boldsymbol{S}_d\} P\{s \in \boldsymbol{S}_d\},
\end{aligned} \tag{11}$$

where $\hat{s}$ is the estimated symbol. Each group-wise term in (11) can be further bounded by its point-wise symbol error probabilities. For example, the symbol error probability for group a can be bounded by

$$\begin{aligned}
&P\{\hat{s} \notin \boldsymbol{S}_a | s \in \boldsymbol{S}_a\} P\{s \in \boldsymbol{S}_a\} \\
&\quad \le \sum_{i=1,4,13,16} P\{\hat{s} \neq s_i | s = s_i\} P\{s = s_i\}.
\end{aligned} \tag{12}$$

Since the constellation is a square QAM-like shape, we can easily calculate the symbol error probability. The constellation can be separated into nine detection areas whose boundaries are shown as the dashed lines in Fig. 4. There are four areas with one point, four for two points, and one for four points.

Lemma 1. The transformed noise n is complex symmetric complex Gaussian (CSCG) and its one-dimensional variance $\sigma_n^2 = \|\boldsymbol{aG}\|^2 N_0/2$.

Proof: $n = \boldsymbol{aGz} = (a_1g_{11} + a_2g_{21})z_1 + (a_1g_{12} + a_2g_{22})z_2$, where g_{ij} is the element in the i-th row and j-th column of $\boldsymbol{G}$ and $\boldsymbol{z} = [z_1\ z_2]$. Since z_j is CSCG, $(a_1g_{1j} + a_2g_{2j})z_j$ is CSCG too. Therefore, n is a sum of two CSCG random variables, and thus is also CSCG.

Hence, $\mu_n = 0$ and $\sigma_n^2 = [(a_1g_{11} + a_2g_{21})^2 + (a_1g_{12} + a_2g_{22})^2]N0/2 = \|\boldsymbol{aG}\|^2 N_0/2$ ■

To calculate the overall symbol error rate P_e, we first consider the correct detection probability of one particular symbol, i.e., $P\{\hat{s} = s_i | s = s_i\}, i = 1, \ldots, 16$. It is easy to see that the correct detection probability for the points within a given group are the same. Denote P_a, P_b, P_c, and P_d the correct detection probabilities for the four groups respectively. For example, $P_b = P\{\hat{s} = s_i | s = s_i\}, i = 2, 3, 14,$ and 15. By inspecting the superimposed constellation and the fact that n

is CSCG, we can write the four correct detection probabilities as

$$\begin{aligned}
P_a &= \left[1 - Q\left(\frac{a_m d}{2\sigma_n}\right)\right]^2 \\
P_b &= \left[1 - Q\left(\frac{a_m d}{2\sigma_n}\right) - Q\left(\frac{(2a_M - a_m)d}{2\sigma_n}\right)\right] \cdot \\
&\quad \left[1 - Q\left(\frac{a_m d}{2\sigma_n}\right)\right] \\
P_c &= \left[1 - Q\left(\frac{a_m d}{2\sigma_n}\right) - Q\left(\frac{(2a_M - a_m)d}{2\sigma_n}\right)\right] \cdot \\
&\quad \left[1 - Q\left(\frac{a_m d}{2\sigma_n}\right)\right] \\
P_d &= \left[1 - Q\left(\frac{a_m d}{2\sigma_n}\right) - Q\left(\frac{(2a_M - a_m)d}{2\sigma_n}\right)\right]^2 .
\end{aligned} \tag{13}$$

Note that $P_b = P_c$, since the points in $\boldsymbol{S}_b$ and $\boldsymbol{S}_c$ have similar geometric locations in the constellation. Thus the error detection probability $P\{\hat{s} \neq s_i | s = s_i\} = 1 - P_a$ if $s_i \in \mathcal{S}_a$, and so on. From (11) and (12), the symbol error rate can be shown as

$$\begin{aligned}
P_e \leq & 4 \times \frac{1}{16} \times (1 - P_a) + 4 \times \frac{1}{16} \times (1 - P_b) + \\
& 4 \times \frac{1}{16} \times (1 - P_c) + 4 \times \frac{1}{16} \times (1 - P_d).
\end{aligned} \tag{14}$$

Let E_s be the average transmitted symbol energy for both end nodes. We have $d = \sqrt{2E_s}$. From Lemma 1, the two forms of Q-function terms in (13) can be written as

$$Q\left(\frac{a_m d}{2\sigma_n}\right) = Q\left(\sqrt{\left(\frac{a_m^2}{\|\boldsymbol{aG}\|^2}\right)\frac{E_s}{N_0}}\right) \tag{15}$$

$$Q\left(\frac{(2a_M - a_m)d}{2\sigma_n}\right) = Q\left(\sqrt{\left(\frac{(2a_M - a_m)^2}{\|\boldsymbol{aG}\|^2}\right)\frac{E_s}{N_0}}\right). \tag{16}$$

By substituing (15) and (16) into (13), we can obtain the relationship between the linear combiner $\boldsymbol{a}$ and the symbol error rate.

3) To Obtain Optimized $\boldsymbol{a}$: The linear combiner $\boldsymbol{a}$ plays an important role in our method. The restriction that $\boldsymbol{a}$ is real keeps the superimposed constellation a square QAM-like shape. Hence, its symbol error rate can be obtained very easily. Furthermore, choosing an optimized value of $\boldsymbol{a}$ can further result in better performance. From the SER bound in (14), we can minimize the right-hand-side value to get better SER. Thus, we calculate the optimized $\boldsymbol{a}$ by minimizing the right-hand-side in (14), for which relationship with $\boldsymbol{a}$ is obtained from (15) and (16).

To minimize the right-hand-side, we have to minimize the Q-function terms in $P_a, P_b, P_c,$ and P_d. There are two forms

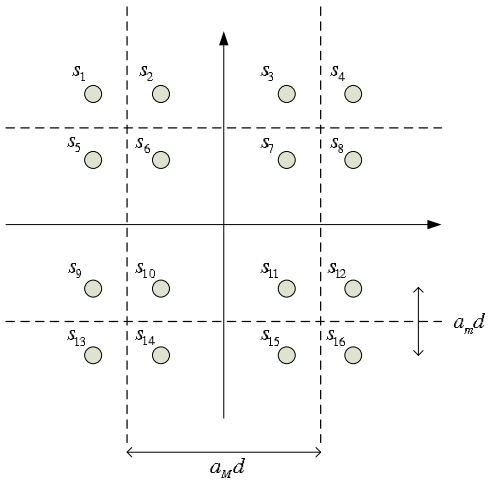

Fig. 4. Superimposed constellation $\boldsymbol{ax}$ for $\boldsymbol{a} = [a_1\ a_2]$, where $a_m = \min\{|a_1|, |a_2|\}$, $a_M = \max\{|a_1|, |a_2|\}$, and d is the minimum distance of each component constellation. The dashed lines represent the detection boundaries.

of the Q functions:

$$Q\left(\sqrt{\left(\frac{a_m^2}{\|\boldsymbol{aG}\|^2}\right)\frac{E_s}{N_0}}\right) \tag{17}$$

$$Q\left(\sqrt{\left(\frac{(2a_M - a_m)^2}{\|\boldsymbol{aG}\|^2}\right)\frac{E_s}{N_0}}\right). \tag{18}$$

We choose (17) as the target for minimization. Since $a_m^2 \leq (2a_M - a_m)^2$, we always have

$$Q\left(\sqrt{\left(\frac{a_m^2}{\|\boldsymbol{aG}\|^2}\right)\frac{E_s}{N_0}}\right) \geq Q\left(\sqrt{\left(\frac{(2a_M - a_m)^2}{\|\boldsymbol{aG}\|^2}\right)\frac{E_s}{N_0}}\right).$$

Thus (17) should be a dominant term between the two. Therefore, the optimized $\hat{\boldsymbol{a}}$ is obtained by

$$\hat{\boldsymbol{a}} = \arg\max_{\boldsymbol{a}} \frac{a_m^2}{\|\boldsymbol{aG}\|^2}. \tag{19}$$

Let $\boldsymbol{u} = [u_1\ u_2] = [a_1/a_m\ \ a_2/a_m]$. Then $a_m^2/\|\boldsymbol{aG}\|^2 = 1/\|\boldsymbol{uG}\|^2$. Since a_m is the minimum value between $|a_1|$ and $|a_2|$, we have either $|u_1| = 1$ or $|u_2| = 1$. Furthermore, if $|u_1| = 1$, then $|u_2| = a_M/a_m \geq 1$, and vice versa. We can formulate our optimization problem as

$$\begin{aligned}
\text{minimize} \quad & \|\boldsymbol{uG}\|^2 \\
\text{subject to} \quad & (|u_1| = 1 \text{ and } |u_2| \geq 1) \text{ or} \\
& (|u_2| = 1 \text{ and } |u_1| \geq 1).
\end{aligned} \tag{20}$$

We can solve this problem by considering the four cases: $u_1 = \pm 1$ and $u_2 = \pm 1$. If $u_1 = 1$,

$$\begin{aligned}
\|\boldsymbol{uG}\|^2 &= \boldsymbol{uGG}^*\boldsymbol{u}^* \\
&= [1\ u_2] \begin{bmatrix} p & q \\ q* & r \end{bmatrix} \begin{bmatrix} 1 \\ u_2 \end{bmatrix} \\
&= p + (q + q^*)u_2 + ru_2^2 \\
&= r(u_2 + \frac{q + q^*}{2r})^2 + \frac{4pr - (q + q^*)^2}{4r},
\end{aligned} \tag{21}$$

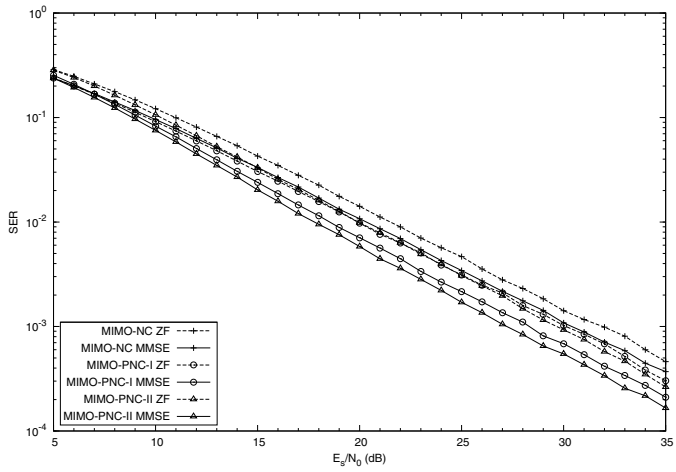

Fig. 5. Simulation results of MIMO-NC, MIMO-PNC-I and MIMO-PNC-II.

where p, q, q^*, and r are entries in $\boldsymbol{G}\boldsymbol{G}^*$. p and r are real and non-negative since $\boldsymbol{G}\boldsymbol{G}^*$ is positive semidefinite. The parameter u_2 and the minimal $\|\boldsymbol{u}\boldsymbol{G}\|^2$ are

$$\begin{cases} \|\boldsymbol{u}\boldsymbol{G}\|^2 = \frac{4pr-(q+q^*)^2}{4r},\ u_2 = -\frac{q+q^*}{2r} & \text{if } |-\frac{q+q^*}{2r}| \geq 1 \\ \|\boldsymbol{u}\boldsymbol{G}\|^2 = p+r+(q+q^*),\ u_2 = 1 & \text{if } 0 \leq -\frac{q+q^*}{2r} < 1 \\ \|\boldsymbol{u}\boldsymbol{G}\|^2 = p+r-(q+q^*),\ u_2 = -1 & \text{if } -1 < -\frac{q+q^*}{2r} < 0 \end{cases} \tag{22}$$

Similar results can be derived from the other three cases:
If $u_1 = -1$,

$$\begin{cases} \|\boldsymbol{u}\boldsymbol{G}\|^2 = \frac{4pr-(q+q^*)^2}{4r},\ u_2 = \frac{q+q^*}{2r} & \text{if } |\frac{q+q^*}{2r}| \geq 1 \\ \|\boldsymbol{u}\boldsymbol{G}\|^2 = p+r-(q+q^*),\ u_2 = 1 & \text{if } 0 \leq -\frac{q+q^*}{2r} < 1 \\ \|\boldsymbol{u}\boldsymbol{G}\|^2 = p+r+(q+q^*),\ u_2 = -1 & \text{if } -1 < -\frac{q+q^*}{2r} < 0 \end{cases} \tag{23}$$

If $u_2 = 1$,

$$\begin{cases} \|\boldsymbol{u}\boldsymbol{G}\|^2 = \frac{4pr-(q+q^*)^2}{4p},\ u_1 = -\frac{q+q^*}{2p} & \text{if } |-\frac{q+q^*}{2p}| \geq 1 \\ \|\boldsymbol{u}\boldsymbol{G}\|^2 = p+r+(q+q^*),\ u_1 = 1 & \text{if } 0 \leq -\frac{q+q^*}{2r} < 1 \\ \|\boldsymbol{u}\boldsymbol{G}\|^2 = p+r-(q+q^*),\ u_1 = -1 & \text{if } -1 < -\frac{q+q^*}{2r} < 0 \end{cases} \tag{24}$$

If $u_2 = -1$,

$$\begin{cases} \|\boldsymbol{u}\boldsymbol{G}\|^2 = \frac{4pr-(q+q^*)^2}{4p},\ u_1 = \frac{q+q^*}{2p} & \text{if } |\frac{q+q^*}{2p}| \geq 1 \\ \|\boldsymbol{u}\boldsymbol{G}\|^2 = p+r-(q+q^*),\ u_1 = 1 & \text{if } 0 \leq -\frac{q+q^*}{2r} < 1 \\ \|\boldsymbol{u}\boldsymbol{G}\|^2 = p+r+(q+q^*),\ u_1 = -1 & \text{if } -1 < -\frac{q+q^*}{2r} < 0 \end{cases} \tag{25}$$

We choose the optimal $\hat{\boldsymbol{u}}$ which can produce the smallest $\|\boldsymbol{u}\boldsymbol{G}\|^2$. Finally, we choose $\hat{\boldsymbol{a}} = a_m \cdot \hat{\boldsymbol{u}} = \hat{\boldsymbol{u}}$. Since a_m does not affect the value of $a_m^2/\|\boldsymbol{a}\boldsymbol{G}\|^2$, we set $a_m = 1$ for convenience.

IV. Simulation Results

A. Simulation Results

In this section, we show the performance of our proposed method, i.e., MIMO-PNC-II. Also, performance of MIMO-NC and MIMO-PNC-I are also shown as comparison. The system is modelled according to the discussion in Section II. Both end nodes use Gray-labelled QPSK for their transmitted symbols. Block Rayleigh fading is adopted and each entry in H is a complex Gaussian random variable with zero mean and variance N_0, i.e., $h_{ij} \sim \mathcal{CN}(0, N_0)$. For the simulation of MIMO-PNC [5], we extend the scheme to QPSK by independently detecting the real and imaginary parts of symbols.

Fig. 5 shows the performance results. For ZF-based schemes, our proposed ZF-based scheme outperforms MIMO-NC scheme by about 2 dB at SER of 10^{-3}. However, there is negligible performance gain between our method and MIMO-PNC-I. For MMSE-based schemes, our method outperforms MIMO-NC by about 3 dB. There is also 1 dB gain as compared to MIMO-PNC-I. Note that MIMO-PNC-I is similar to set $\boldsymbol{a} = [1\ 1]$ and $[1\ \ -1]$ in our scheme. However, some channel conditions may favor other $\boldsymbol{a}$ values which can provide further performance gain. The performance gain brought by an optimized $\boldsymbol{a}$ would become more evident in the MMSE-based schemes.

V. Conclusion

In this paper, we proposed a PNC mapping scheme which is based on the MIMO linear detection. In addition to a linear detector, a linear combiner $\boldsymbol{a}$ is introduced to control the combination of the two component constellations. We propose to use the real-valued $\boldsymbol{a}$ which keeps the superimposed constellation a square QAM-like shape so that the symbol error rate can be easily derived. Furthermore, we provided a simple method to find an optimized $\boldsymbol{a}$, which can provide better performance than using a sum/difference constellation only.

References

[1] R. Ahlswede, N. Cai, S.-Y. R. Li, and R. W. Yeung, "Network information flow," *IEEE Trans. Inf. Theory*, vol. 46, no. 4, pp. 1204–1216, Jul. 2000.

[2] C. Fragouli, J. Y. Boudec, and J. Widmer, "Network coding: An instant primer," *ACM SIGCOMM Computer Communication Review*, vol. 36, no. 1, pp. 63–68, Jan. 2006.

[3] S. Zhang, S. C. Liew, and P. P. Lam, "Hot topic: physical-layer network coding," in *in Proc. of ACM Mobicom*, 2006, pp. 358–365.

[4] D. Xu, Z. Bai, A. Waadt, G. H. Bruck, and P. Jung, "Combining MIMO with network coding: A viable means to provide multiplexing and diversity in wireless relay networks," in *Proc. IEEE ICC 2010*.

[5] S. Zhang and S. C. Liew, "Physical layer network coding with multiple antennas," in *Proc. IEEE WCNC 2010*.

[6] K.-A. Toshiaki, P. Popovski, and V. Tarokh, "Optimized constellations for two-way wireless relaying with physical network coding," *IEEE J. Sel. Areas Commun.*, vol. 27, no. 5, pp. 773–787, Jun. 2009.

[7] D. Tse and P. Viswanath, *Fundamentals of Wireless Communication*. Cambridge University Press, 2005.